ACS APPLIED MATERIALS & INTERFACES

Research Article

Cite This: ACS Appl. Mater. Interfaces XXXX, XXX, XXX−XXX

www.acsami.org

Existence of Solid Electrolyte Interphase in Mg Batteries: Mg/S Chemistry as an Example

Tao Gao, Singyuk Hou, Khue Huynh, Fei Wang, Nico Eidson, Xiulin Fan, Fudong Han, Chao Luo, Minglei Mao, Xiaogang Li, and Chunsheng Wang*

Chemical and Biomolecular Engineering, University of Maryland, College Park, Maryland 20740, United States

Supporting Information

ABSTRACT: Magnesium redox chemistry is a very appealing "beyond Li ion chemistry" for realizing high energy density batteries due to the high capacity, low reduction potential, and most importantly, highly reversible and dendrite-free Mg metal anode. However, the progress of rechargeable Mg batteries has been greatly hindered by shortage of electrolytes with wide stability window, high ionic conductivity, and good compatibility with cathode materials. Unlike solid electrolyte interphase on Li metal anode, surface film formed by electrolyte decomposition in Mg batteries was considered to block Mg ion transport and passivate Mg electrode. For this reason, the attention of the community has been mainly focusing on surface layer free electrolytes, while reductively unstable salts/solvents are barely considered, despite many of them possessing all the necessary properties for good electrolytes. Here, for the first time, we demonstrate that the surface film formed by electrolyte decomposition can function as a solid electrolyte interphase (SEI). Using Mg/S chemistry as a model system, the SEI formation mechanism on Mg metal anode was thoroughly examined using electrochemical methods and surface chemistry characterization techniques such as EDX and XPS. On the basis of these results, a comprehensive view of the Mg/electrolyte interface that unifies both the SEI mechanism and the passivation layer mechanism is proposed. This new picture of surface layer on Mg metal anode in Mg batteries not only revolutionizes current understanding of Mg/electrolyte interface but also opens new avenues for electrolyte development by uncovering the potential of those reductively unstable candidates through interface design.

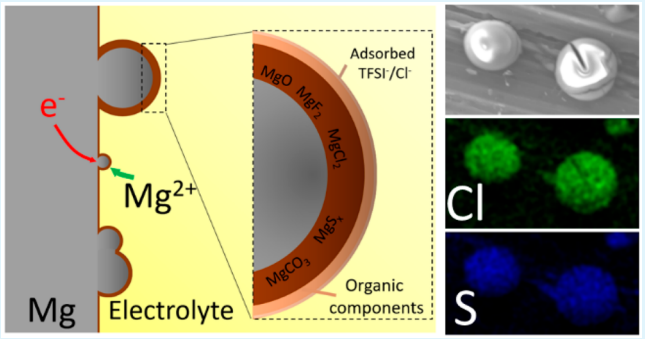

KEYWORDS: *magnesium battery, sulfur, electrolyte, solid electrolyte interphase, electrochemistry, surface chemistry*

INTRODUCTION

High capacity (2205 mAh/g and 3833 mAh/cm^3), low reduction potential (−2.36 V vs SHE), high abundance, and highly reversible (100%) deposition/striping in certain electrolytes with no dendrite formation have made Mg metal an ideal anode for high energy density rechargeable metal batteries.[1] To utilize its great potential, the first rechargeable Mg metal battery was successfully prototyped in 2001.[2] Since then, lots of efforts were made to improve the energy density of rechargeable Mg batteries.[3−15] On the other hand, continuous endeavors were also devoted to developing electrolytes with wide stability window, good compatibility with cathode materials, and high ionic conductivity.[16,17]

Due to Mg's low redox potential, electrolytes are susceptible to reduction in the vicinity of Mg metal, leading to the formation of a solid film covering the Mg electrode surface.[18] It is believed any such surface films would block the transport of Mg^{2+} and passivate the Mg anode due to the sluggish transport of Mg^{2+} in the solid phase.[18] Hence, research on Mg electrolytes has mainly focused on synthesizing salts (either Lewis acid−base complex salts[19−21] or salts with bulky weakly coordinating anions[22,23]) that are stable to Mg and soluble in ethereal solvent (the only viable organic solvents inert to Mg electrode).[24] However, recent study showed reversible Mg deposition/striping is possible even with the presence of surface film, for example, in $MgTFSI_2$-glyme electrolyte.[25−27] Another example that contradicts the passivation mechanism is rechargeable Mg/S batteries.[28−30] In Mg/S batteries, soluble polysulfide species form during discharge[31,32], and they are prone to react with Mg anode. If a passivation surface layer is formed, Mg anode should fail or at least demonstrate very large overpotential to drive the deposition/striping reaction. However, the Mg/S battery can actually operate with a small hysteresis at a discharge voltage (1.5−1.6 V) close to the theoretical voltage (1.77 V).[28,29] Both observations have challenged the long-held passivation mechanism of Mg/electrolyte interface. Because the electrolyte and its interface with Mg anode play a determining role in the reversibility of rechargeable Mg batteries, a comprehensive understanding of the Mg/electrolyte interface is in urgent demand to explain the

Received: February 8, 2018
Accepted: April 5, 2018
Published: April 5, 2018

DOI: 10.1021/acsami.8b02425
ACS Appl. Mater. Interfaces XXXX, XXX, XXX−XXX

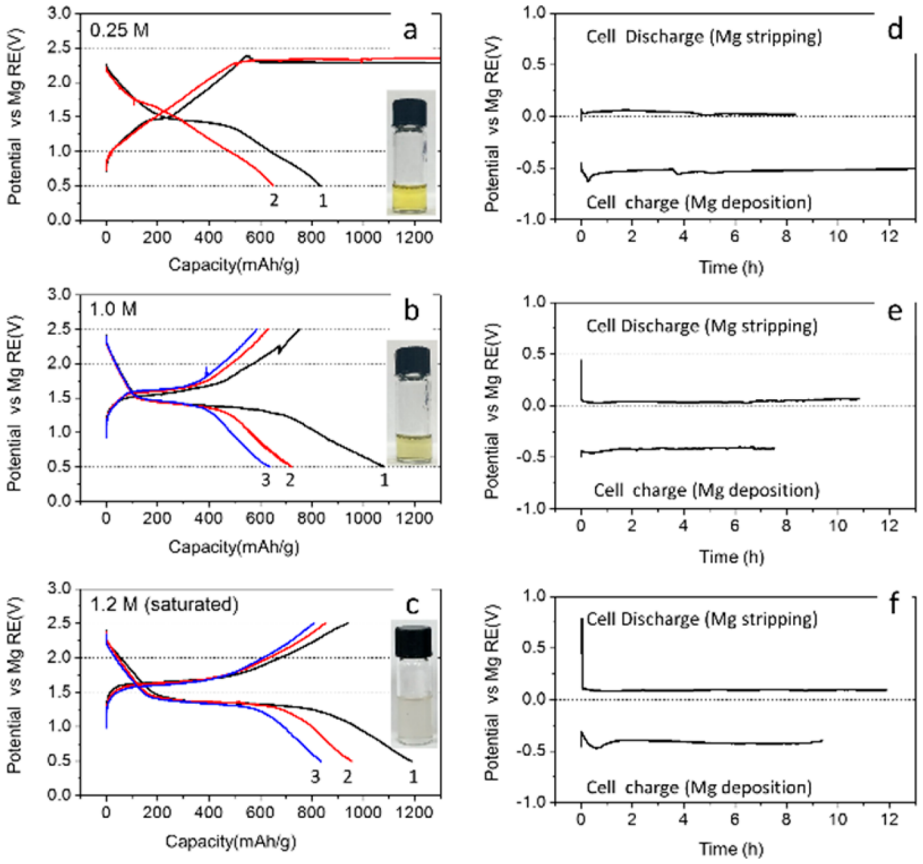

Figure 1. Electrochemical results of three-electrode Mg/S cells. (a–c) Potentials of S cathode vs Mg reference electrode (RE) in $MgTFSI_2$–$MgCl_2$–DME electrolytes with different concentrations. Inset: the color of the electrolyte after first discharge. Current: 100 mA/g. S loading: ~1.0 mg/cm^2. Potential: 0.5–2.5 V. Cell with 0.25 M electrolyte is charged for 17 h before cutoff. (d–f) Potentials of Mg anode vs Mg RE, 1st cycle.

discrepancies as well as to provide guidance for electrolyte development and interface design.

In this study, for the first time, we conducted a systematic investigation on the Mg/electrolyte interface using Mg/S battery as a model system. By thoroughly examining the electrochemistry and surface chemistry of Mg electrodes, we demonstrated the formation of solid electrolyte interphase (SEI) on Mg electrode. On the basis of the surface layer formation mechanism and its electronic/ionic transport properties, we propose a comprehensive view of Mg/electrolyte interface. This view is able to unify both the passivation mechanism, where the surface film cannot conduct Mg^{2+} so Mg anode fails, and the SEI mechanism, where the surface film can conduct Mg^{2+} under mild overpotential driving force hence Mg anode can work reversibly. This understanding of Mg/electrolyte interface not only explains the discrepancies mentioned above but also opens a new avenue for electrolyte development through interface design in the future.

RESULTS

To reveal the SEI formation in Mg/S battery, we first examined how the reaction of the dissolved sulfur species with Mg influences the electrochemistry of Mg electrode. The potential of both S cathode and Mg anode (Figure 1) and capacities of Mg/S cell (Figure S1) in electrolytes of different concentrations were evaluated in a three-electrode cell (Figure S2). The discharge curves of S cathode are in good agreement with our previous mechanistic study on the reaction pathway of S in Mg chemistry.[32] Three stages were observed: a slope (OCP-1.5 V), a plateau (~1.5 V), and another slope (1.5–0.5 V), corresponding to the formation of long-chain polysulfide, long-chain to short-chain polysulfide transition, and short-chain polysulfide to MgS transition, respectively. The charging curves share a similar three-stage pattern, corresponding to the reverse process of the above-mentioned reactions, yet the charging in 0.25 M shows a unique long plateau at 2.3 V (Figure 1a), indicative of the polysulfide shuttle effect.[33] The dissolution of polysulfide is also evidenced by the colorimetric change of the electrolyte after the first discharge (from colorless to yellow) (inset of Figures 1a–c). Increasing electrolyte concentration can mitigate polysulfide dissolution as evidenced by fading color, consistent with our previous study.[31] It is important to point out that the active material loss due to the dissolution of polysulfide has a direct influence on the first discharge capacity, manifested by the shortening of the potential plateau at ~1.5 V: at high concentration (1.2 M), nearly all capacity (~800 mAh/g) corresponding to the formation of long-chain polysulfide (stage I) and its shortening to MgS_2 (stages II) is delivered,[32] but only ~500 mAh/g is delivered at the lower concentration (0.25 M). As a result, the cells deliver 826, 1016, and 1187 mAh/g, respectively in the 0.25, 1.0, and 1.2 M electrolytes. The mitigation of polysulfide dissolution and the slow mass transport in the more viscous solutions have inhibited the shuttle effect in concentrated electrolytes (1.0 and 1.2 M), leading to the absence of long shuttle effect plateaus at the end of the charge (nearly 100% Coulombic efficiency starting from 3nd cycle).

DOI: 10.1021/acsami.8b02425
ACS Appl. Mater. Interfaces XXXX, XXX, XXX–XXX

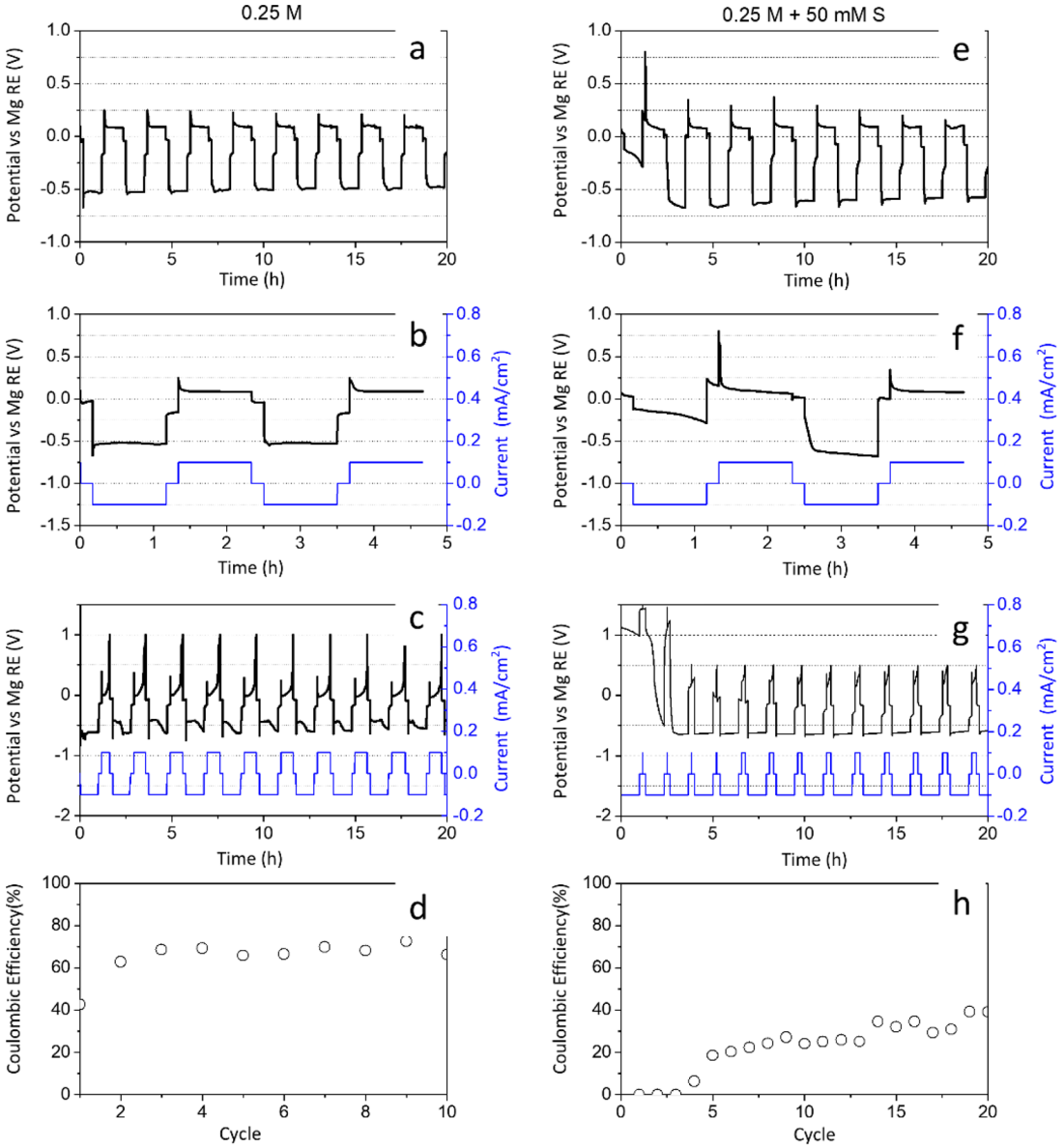

Figure 2. Three-electrode cells cycled in blank electrolyte and electrolyte dissolved with sulfur. Left: blank electrolyte with no sulfur (0.25 m). Right: sulfur containing electrolyte (0.25 M + 50 mM S). (a and e) Potentials of Mg WE in the first 20 h and (b and f) in the first 5 h in Mg/Mg/Mg three-electrode cells. Current: 0.1 mA/cm^2. Both discharge and charge are cut off at 1 h. (c and g) Potentials of Pt WE vs Mg RE and (d and h) Coulombic efficiencies of Mg deposition/striping in Pt/Mg/Mg three-electrode cells. Current: 0.1 mA/cm^2. Discharge is cut off at 1 h and charge is cut off at 1.0 V in the blank electrolyte and 0.5 V in the sulfur containing electrolyte to avoid the oxidation of any formed MgS_x surface layer.

As for Mg anode, positive potential is required to drive Mg striping (cell discharge), and negative potential is required to drive Mg deposition (cell charge) (Figures 1d–f). The striping/deposition overpotential are asymmetrical, as striping requires only <0.1 V overpotential, but deposition needs 0.4–0.5 V in all electrolyte concentrations.[25] Nevertheless, surface passivation resulted from the reduction of dissolved sulfur species, which would exert a large overpotential for striping/deposition,[24,26] is unlikely to happen given all the stripping overpotentials are very small (<0.1 V).

To understand how the dissolved sulfur species (polysulfide + elemental sulfur) affect the reaction kinetics of the Mg electrode, the electrochemical behavior of Mg electrode in 0.25 M $MgTFSI_2$–$MgCl_2$–DME electrolyte dissolved with 50 mM sulfur was studied. Galvanostatic discharge/charge experiments were performed with Mg/Mg/Mg three-electrode cells in both the blank electrolyte (Figures 2a and b) and sulfur containing electrolyte (Figures 2e and f). Consistent with Figures 1d and f, both cells show asymmetrical overpotentials, which gradually stabilize to −0.48/0.09 V (discharging/charging) in the blank electrolyte (Figure 2a) and −0.58/0.11 V in the sulfur containing electrolyte (Figure 2e), suggesting the operation of the Mg electrode is only slighted impeded in the presence of sulfur. This hindered kinetics suggests the presence of a surface layer on Mg in the sulfur containing electrolyte, whose formation is manifested by the unique discharge profile in the first two cycles (Figures 2b and f), as explained below.

In the blank electrolyte, the potential jumps down from open circuit potential (OCP) upon discharge and instantaneously reaches the plateau for deposition (−0.5 V) after a nucleation dip (Figure 2b), while in the sulfur containing electrolyte, the potential decreases gradually and does not attain any plateau in

DOI: 10.1021/acsami.8b02425
ACS Appl. Mater. Interfaces XXXX, XXX, XXX−XXX

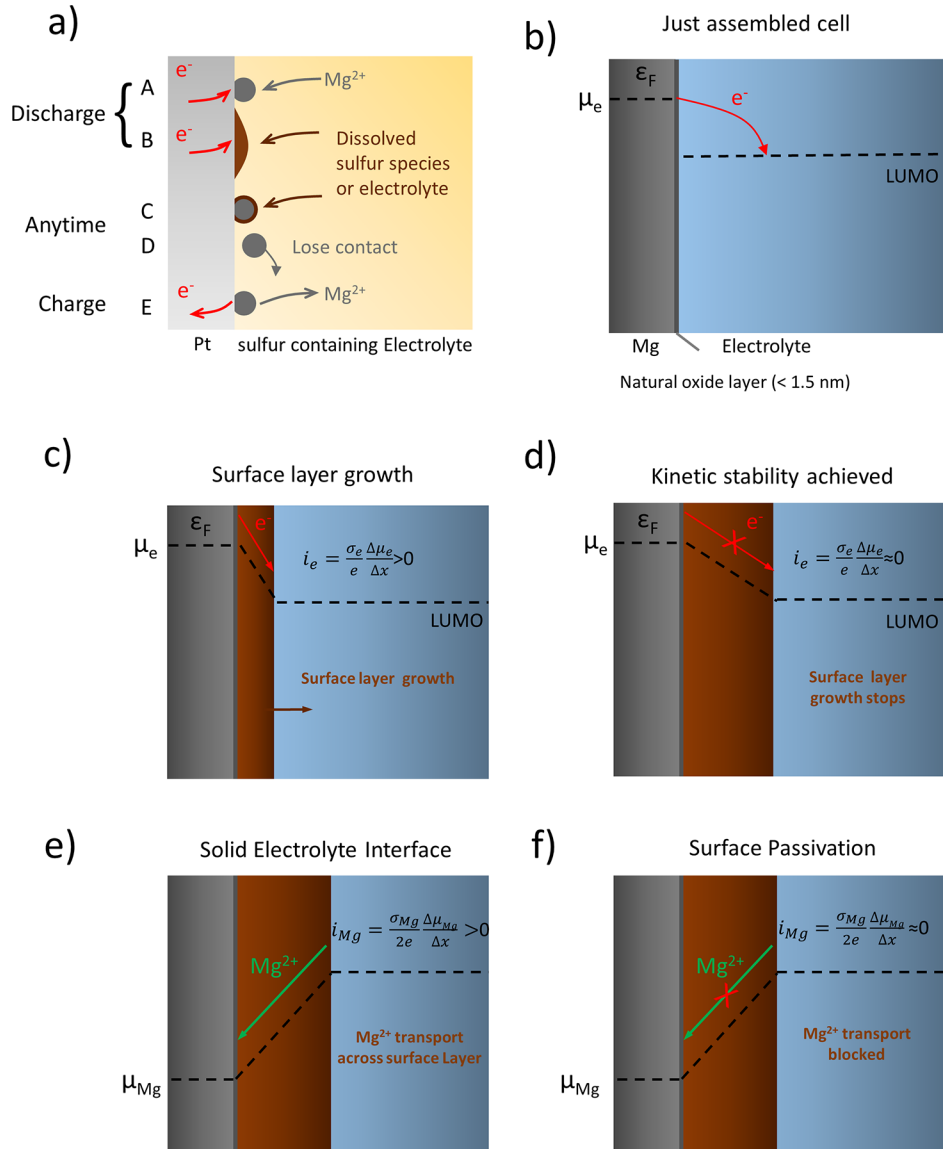

Figure 3. (a) Reactions occurring at the Pt/Mg electrolyte interface. A: Reduction of Mg^{2+} to Mg. B: Reduction of electrolyte or any dissolved species. C: Chemical reaction between Mg deposits with electrolyte or any dissolved species. D: Mg deposits losing contact with the substrate. E: Oxidation of Mg to Mg^{2+}. b-d) Formation of surface layer. The growth of surface layer stops when the electronic current i_e decreases to a negligible level so that no reduction reaction occurs. μ_e: electrochemical potential of electrons. ε_F: Fermi energy of Mg electrode. LUMO: the lowest unoccupied molecular orbit of the electrolyte. σ_e: electronic conductivity of the surface layer. i_e: electronic current. Δx: the thickness of the surface layer. (e) Surface layer functions as SEI). (f) Surface layer passivates Mg electrode. μ_{Mg}: electrochemical potential of Mg^{2+}. σ_{Mg}: ionic conductivity of the surface layer. i_{Mg}: ionic current. If the ionic current i_{mg} is zero at the applied overpotential, Mg electrode is passivated.

the first discharge (Figure 2f). Such peculiar potential profile implies the reduction of dissolved sulfur species at the Mg surface upon discharge, further supported by the formation of soluble polysulfide (Figure S3). The potential continues its decreasing trend in the second discharge until reaching a plateau at −0.58 V, where Mg deposition is eventually triggered. In contrast to the Mg WE, the potential of the Mg counter electrode (CE) displays normal Mg striping features during first discharge (Figure S4). Nonetheless, similar potential profile is observed when the current is reversed, and the reaction on the Mg CE is switched from oxidation to reduction. These results suggest that sulfur species compete with Mg^{2+} for reduction reaction, but not for oxidation reaction. This can be understood from the redox potentials of Mg electrodes and sulfur species: oxidation of Mg (Mg stripping, ≥0.1 V, Figure 2a) precedes oxidation of MgS_x (~1.5 V, Figures 1a−c), while reduction of S and MgS_x (~1.5 V) precedes reduction of Mg^{2+} (Mg deposition, ≤ −0.5 V, Figure 2a).

Because the reduction of sulfur species is an undesirable side reaction, its presence inevitably undermines the reversibility of the Mg anode. Galvanostatic discharge/charge with Pt/Mg/Mg three-electrode cells were performed to quantify the reversibility by calculating the Coulombic efficiencies (Figures 2c, d and g, h). The Coulombic efficiency for Mg stripping/plating in electrolytes with and without S additive can be explained with the schematic reaction mechanism (Figure 3). Ideally (100% Coulombic efficiency), only Mg deposition occurs during discharge (Figure 3a, A), and during the subsequent charge, all the deposits can be stripped (Figure 3a, E). The Coulombic efficiency can be compromised by two processes: (1) the presence of a competing electrochemical reduction reaction

DOI: 10.1021/acsami.8b02425
ACS Appl. Mater. Interfaces XXXX, XXX, XXX−XXX

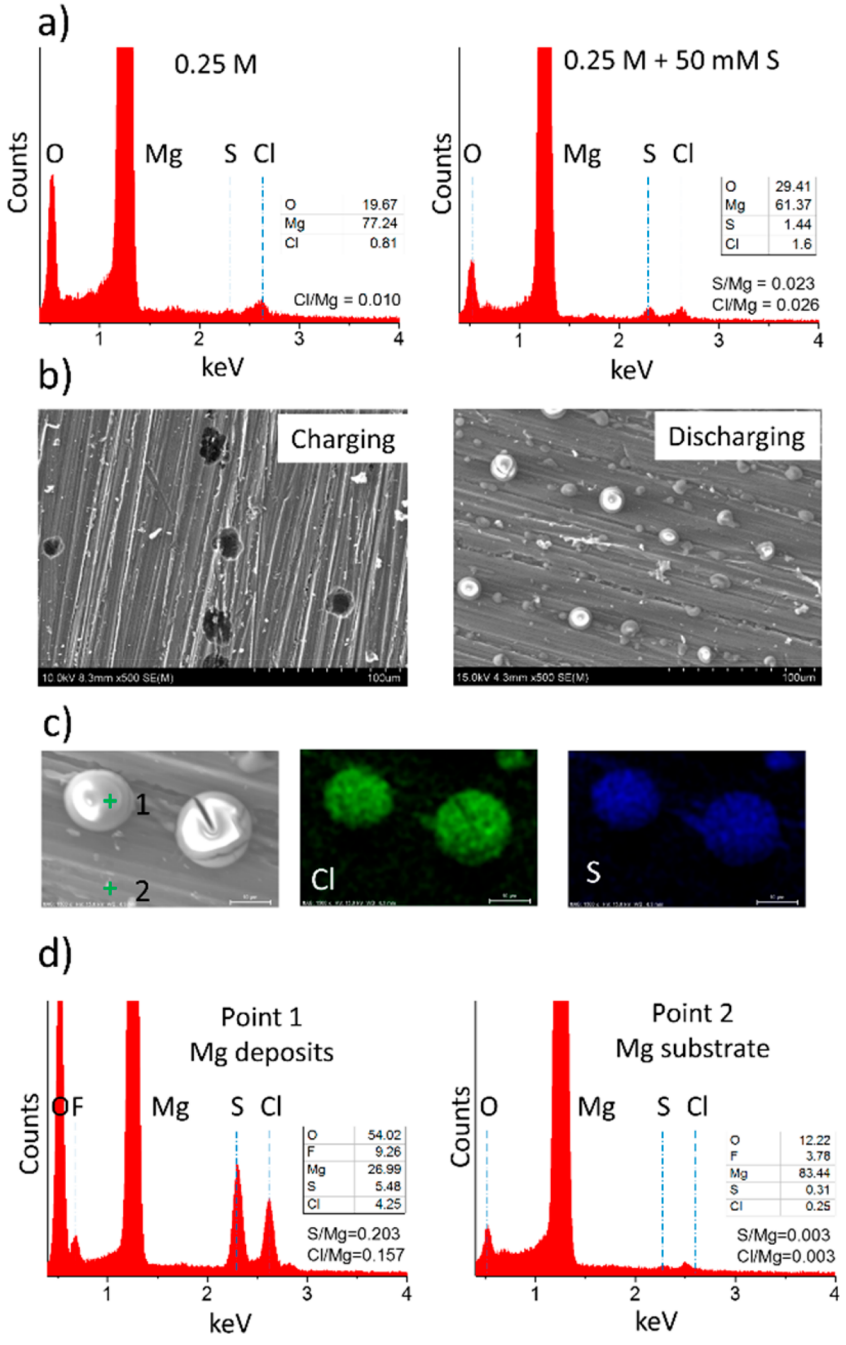

Figure 4. (a) EDX spectra of Mg electrodes recovered from cycled cells. Left: blank electrolyte. Right: sulfur containing electrolyte. (b) Morphology of Mg electrodes charged (oxidized) for 1 h (left) or discharged (reduced) for 3 h (right) in sulfur containing electrolyte. (c) EDX element mapping and (d) EDS point spectra of Mg electrode discharged for 3 h in sulfur containing electrolyte. Current: 0.1 mA/cm^2. Atomic percentage of different elements are given in all EDX spectra. Point 1: Mg deposits. Point 2: Mg substrate.

during discharge (decomposition of electrolyte or reduction of polysulfide species) (Figure 3a, B) or (2) the deposited Mg loses electrochemical activity due to chemical attack by electrolyte or polysulfide (Figure 3a, C) or other factors like loss of electrical contact (Figure 3a, D). In the blank electrolyte, Mg deposition/striping on the Pt substrate occurs at a similar potential as that on the Mg substrate (Figure 2c), and the Coulombic efficiency stabilizes to ~70% during cycling (Figure 2d). It should be noted that we obtain a lower Coulombic efficiency for the $MgTFSI_2$–$MgCl_2$–DME electrolyte than Aurbach's work,[25] mainly because the measurement method is different. When using the same cyclic voltametry method, a similar Coulombic efficiency is observed.[31] In the sulfur containing electrolyte, discharge potential decreases gradually from OCP (1.2 V) in the first two cycles and does not reach any plateau until the third cycle (Figure 2g), consistent with the above observation on Mg electrode (Figure 2f). The zero Coulombic efficiencies in the first two cycles (Figure 2h) are expected because there is no Mg deposition in the discharges (Figure 3a, B). For the third cycle, any deposited Mg must have lost its electrochemical activity so that the Coulombic efficiency is also zero. Nevertheless, Coulombic efficiency starts to increase from the fourth cycle and attains 40% by the 20th

DOI: 10.1021/acsami.8b02425
ACS Appl. Mater. Interfaces XXXX, XXX, XXX−XXX

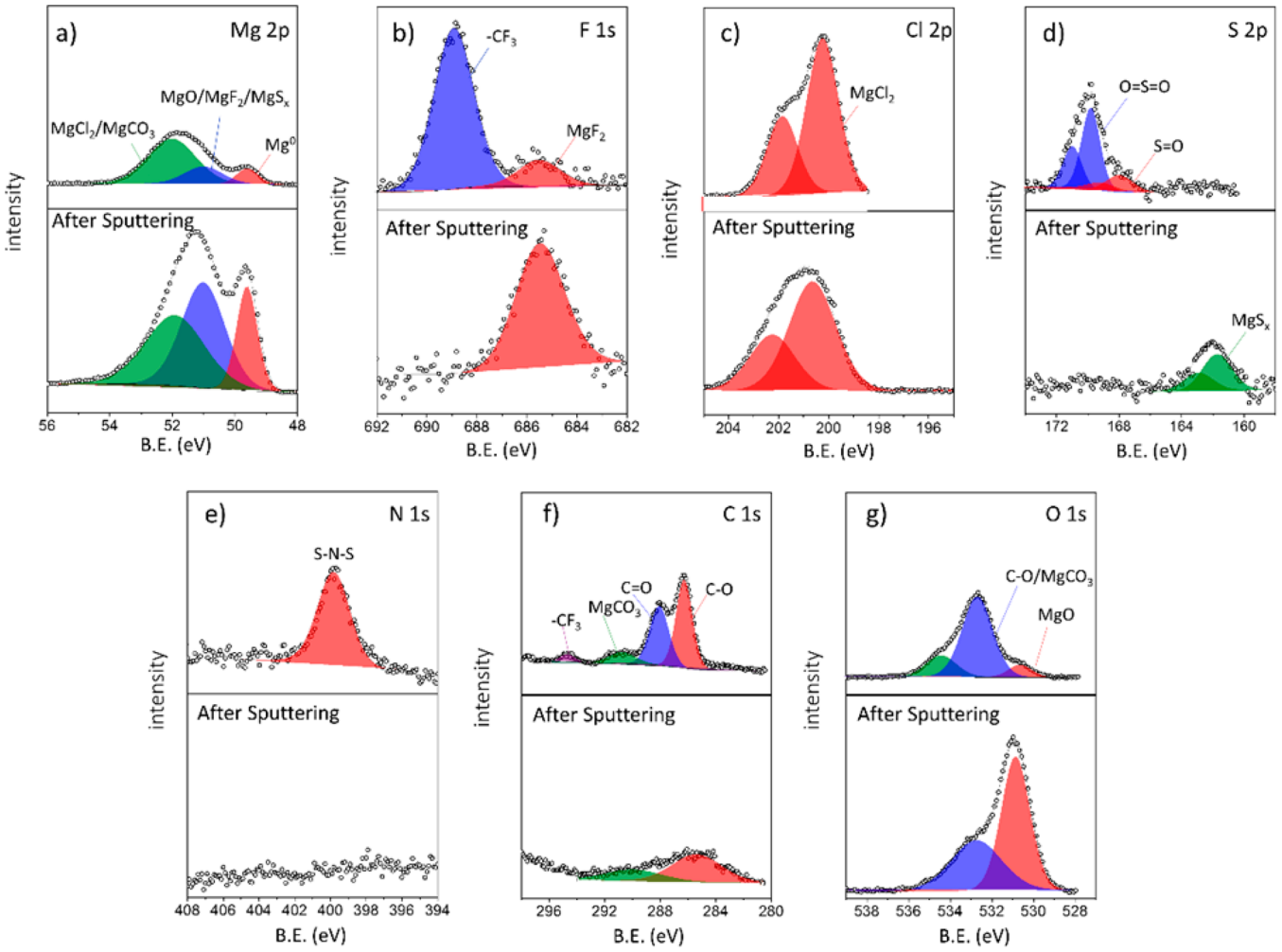

Figure 5. High resolution XPS spectra before (top) and after (bottom) Ar^+ sputtering. (a) Mg 2p, (b) F 1s, (c) Cl 2p, (d) S 2p, (e) N 1s, (f) C 1s, and (g) O 1s. The spectra before and after sputtering are plotted in the same intensity range for comparison. Sputtering time: 10 min.

cycle, indicating a substantial hindrance of the side reaction and enhancement of reversible Mg deposition/striping.

We speculate the gradual improvement of Coulombic efficiency during cycling is due to the covering of the Mg deposit by SEI. This layer blocks direct contact of the deposited Mg with electrolyte, and preferentially conducts Mg^{2+} while impeding the transport of electrons, hence enabling Mg deposition beneath the surface layer while inhibiting the parasitic reduction reactions at the interface. Although it is commonly believed that any surface layer will passivate Mg electrode because Mg^{2+} is difficult to migrate through Mg compounds, this scenario is not comprehensive enough to describe the interface in Mg batteries. In theory, if an electrolyte is not thermodynamically stable with Mg electrode, reduction of the electrolyte occurs at the interface (Figure 3b), and the solid product forms a surface layer. Driven by the energy difference between Fermi level of Mg and electrolyte LUMO (electrochemical potential difference), electrons will migrate through this layer to continue the reduction reaction at the interface (Figure 3c) until the surface layer is thick enough to inhibit the electronic current to a negligible level (Figure 3d) and then kinetic stability of electrolyte is reached. This process occurs spontaneously when the electrolyte is brought to the vicinity of the Mg electrode.[34] The thickness of the surface layer is therefore determined by the driving force (electrochemical potential gradient) and the electronic conductivity. To enable Mg deposition beneath this surface layer, an electrochemical potential gradient must be exerted to drive Mg^{2+} transport across the layer, which can be achieved by applying a negative overpotential on the Mg electrode. If the surface layer is relatively ionic conductive (higher ionic conductivity than electronic conductivity), only a small overpotential is required. In this case, the surface layer functions as an SEI (Figure 3e). If the surface layer is ionic insulating (comparable or even lower ionic conductivity than electronic conductivity), the Mg electrode is practically passivated (Figure 3f) due to the large overpotential. The above discussion describes a general mechanism of the surface layer formation for various anode materials not limited to Mg electrodes. Surface layers in magnesium batteries are commonly believed to be passivation layers, which has explained the failure of Mg electrodes in PC- or AN-based electrolytes.[24] However, this notion contradicts the fact that reversible Mg deposition/striping is possible on Mg electrodes covered by surface layers in some electrolytes.[26,35] Indeed, recent study by Toyota Research Center has provided direct experiment evidence on the presence of SEI on Mg electrode.[36]

To verify the formation of the surface layer and its role as SEI, Mg electrodes cycled in both electrolytes are analyzed by scanning electron microscopy (SEM) and energy dispersive X-

DOI: 10.1021/acsami.8b02425
ACS Appl. Mater. Interfaces XXXX, XXX, XXX−XXX

Table 1. Binding Energies of Possible Species (eV)

species	Mg 2p	O 1s	C 1s	S 2p	F 1s	Cl 2p	N 1s
MgO	1.0[37]	530.8[37]					
	0.8 ± 0.1[38]						
	0.9[39]						
$Mg(OH)_2$	1.0[37]	532.2,[37] 532.1[39]					
	1.0[39]						
$MgCO_3$	2.1[37]	532.7[37]	290.3[37]				
	3.3[40]						
MgS_x	0.9 ± 0.2[b]			161.5[b]			
MgF_2	1.0[41]				685.6[41]		
	1.2 ± 0.1[42]				685.5 ± 0.1[43]		
	1.2 ± 0.1[43]						
$MgCl_2$	2.0,[44]					198.5[44]	
	3.1[45]					200.6[45]	
$TFSI^-$		533.0[46]	293.0[46]	169.4[46]	688.2[47]		399.6[46]
					688.6[46]		

[a]For Mg 2p, only the binding energy differences relative to Mg^0 are given (ΔBE vs Mg metal). The binding energy of Mg^0 is 49.6 eV.[42] Corresponding literatures are listed in the table. Data from different literatures are converted using Au $4f_{7/2}$ of Au (84.0 eV), O 1s of MgO (531.0 eV), and/or C 1s of adventitious carbon (284.8 eV) as common references. [b]The binding energy of polysulfide MgS_x is from experimental data (Figure S9).

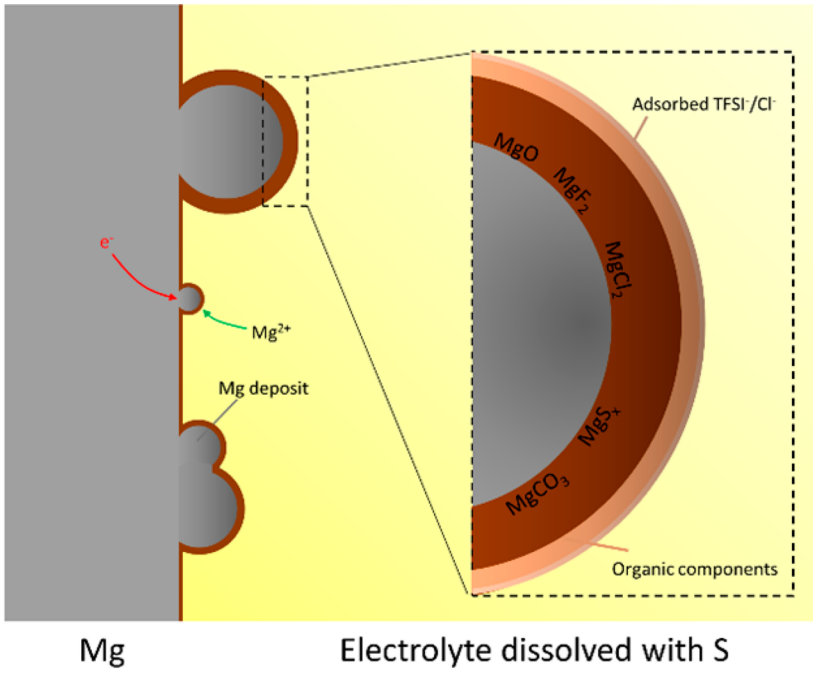

Figure 6. Structure of SEI on Mg electrode cycled in sulfur containing electrolyte.

ray spectra (EDX) (Figure 4, Figure S5). Compared to the Mg electrode cycled in blank electrolyte (Figure 4a, left), the Mg electrode cycled in sulfur containing electrolyte (Figure 4a, right) shows a clear S peak, which suggests reaction between dissolved sulfur species with Mg electrode. The presence of Cl peak could be explained by the adsorption of chlorine from the electrolyte.[25] SEM images show oxidation (charging) of the Mg electrode leaves many holes due to Mg striping (Figure 4b, Figure S6 left), and reduction (discharging) creates spherical deposits. The presence of stripping holes and deposition spheres reaffirms that the Mg electrode is not passivated. EDX element mapping of the deposits (Figure 4c) reveals they are covered by a surface film containing Cl and S, furthered confirmed by the S/Cl peak in the EDX spectra (Figure 4d). The emergence of F peak and the enhanced intensity of O peak suggest this surface film also contains F and O. In comparison to the Mg deposits, no clear S/Cl peak appeared on the Mg substrate, which does not exclude the possibility of the presence of S/Cl on the surface because EDX can fail to detect very thin surface layer due to its detection limit (Figure S5). The presence of S/Cl on the Mg substrate can be detected by X-ray photoelectron spectroscopy (XPS), as we will discuss in next part. Hence, the strong S/Cl/F/O peaks in the EDX spectra of the Mg deposits suggest the newly formed Mg deposits are more prone to the parasitic reaction and surface film formation than the bulk Mg (Mg substrate). In summary, the SEM/EDX result verifies the competing mechanism between Mg deposition and the side reaction at the Mg/electrolyte interface when discharging Mg electrodes in the sulfur containing electrolyte.

DOI: 10.1021/acsami.8b02425
ACS Appl. Mater. Interfaces XXXX, XXX, XXX−XXX

To elaborate on the composition of the surface layer, XPS of Mg electrodes cycled in the sulfur containing electrolyte (the substrate region) was collected (Figure 5). Survey scan shows the presence of Mg, F, Cl, S, O, N, and C peaks (Figure S7), consistent with EDX. These peaks are also observed previously by Aurbach's group[25] and Markovic's group[26] on Mg electrodes cycled in blank electrolyte, suggesting salt decomposition is a major source for the surface layer. Here, we tried to provide a systematic analysis of the structure and composition of the surface layer by carefully fitting the depth profile XPS spectra based on well-accepted XPS spectra positions of different Mg compounds (Table 1).

Two peaks can be explicitly observed in Mg 2p spectra, which reveals the simultaneous presence of Mg^0 (49.6 eV) and Mg compounds (51.2−51.8 eV), suggesting the surface layer is thin.[25,37,26] The amount of Mg increases after sputtering, as evidenced from the enhanced Mg peaks (Figure S8, Figure 5a). Meanwhile, ratio of Mg^0 in Mg 2p spectra increases from 10.7 to 20.0%. Both indicate the thinning of the surface layer by sputtering. To deconvolute the XPS spectra, peak fittings are performed based on the reported binding energies of possible species (Table 1 and Figure S9). Mg 2p spectra are fitted to three separate peaks, given that the binding energies of MgO, $Mg(OH)_2$, MgS_x, and MgF_2 are close (0.8−1.2 eV), and the binding energies of $MgCl_2$ and $MgCO_3$ fall into the same range (1.9−3.3 eV). The presence of $-CF_3$, O═S═O, S═O, and S−N−S peaks can be explained by the adsorption of $TFSI^-$, but the existence of MgF_2 peak suggests its decomposition. Such reduction instability of $TFSI^-$ was predicted in theoretical studies[27,48] and also observed experimentally.[35,26] Sputtering readily removes the adsorbed $TFSI^-$, shown by the vanishing of $-CF_3$, O═S═O, S═O, and S−N−S peaks, and it also exposes more decomposition product of $TFSI^-$ (MgF_2). A polysulfide (MgS_x) peak is seen in S 2p spectrum after sputtering, which evidences the reduction of sulfur species on Mg electrode. The strong Cl signal after sputtering exhibits that $MgCl_2$ is not just adsorbed but also exists as a component of the surface layer. C 1s spectra and O 1s spectra further demonstrate the existence of MgO and $MgCO_3$ in the surface layer. Other than the inorganic compounds (MgF_2, $MgCl_2$, MgS_x, MgO, and $MgCO_3$), organic components are also found from C 1s and O 1s spectra (C═O, C−O), which most likely resides on top of the inorganic species due to the enhanced MgO peak but weakened C−O peak after sputtering.

On the basis the XPS data, the structure of the surface layer is schematically summarized in Figure 6. When the sulfur containing electrolyte is brought to the vicinity to the Mg electrode (substrate), reduction of sulfur and decomposition of electrolyte leads to the formation of surface layer until kinetic stability is achieved. This layer is sufficiently thin to be invisible by EDX but detectable by XPS. During discharge, Mg^{2+} transport through the surface layer at some sites and is reduced, which forms spherical deposits. The volume expansion during the growth of Mg deposits breaks the surface layer, and the reaction of newly deposited Mg^0 with the electrolyte and/or sulfur heals the cracks. Because the newly formed Mg^0 is far more reactive than Mg substrate, surface films on Mg deposits are much thicker than that on the bulk. The surface layer mainly consists of three layers: an inorganic layer containing multiple Mg compounds, a middle layer containing organic components, and an adsorption layer of $TFSI^-/Cl^-$.

CONCLUSION

In conclusion, we reveal that the reduction of sulfur species and electrolyte on the Mg electrode forms a surface layer which does not passivate the Mg electrode and causes its failure, as would be expected from the passivation mechanism. Instead, this surface layer functions as an SEI, which allows Mg^{2+} transport and Mg deposits growth beneath it. The structure and composition of the surface layer is thoroughly investigated through EDX and XPS, and we found it is composed with three layers containing inorganic Mg compounds, organic components, and adsorbed $TFSI^-/Cl^-$, respectively. The reduction of sulfur species produces MgS_x, a component of the SEI, and electrochemical testing demonstrates that the Mg anode in Mg/S battery can work very reversibly with only slightly increased overpotential.

The results presented here has cleared the concern regarding the functionality and reversibility of Mg anode, a critical issue for the practical implementation of Mg/S battery chemistry. The compromised Coulombic efficiency of the Mg electrode can be potentially addressed by inhibiting polysulfide dissolution or tailoring the composition of the surface layer. More importantly, a comprehensive picture of the Mg/electrolyte interface is proposed to elaborate on the mechanism of the surface layer formation, and conditions when it can function as an SEI. This picture not only unifies the current passivation mechanism with our proposed SEI mechanism, which explains the discrepancies in recent experiment studies,[25−30] but also provides new insights in examining the interface in Mg batteries. The understanding regarding surface film on Mg electrode would also enable the design of new electrolytes or additives for better performance by manipulating interfacial chemistry. In our recent work, we set the first step out to explore the possibilities, by using iodine as an additive to enhance the ionic conductivity of the surface film.[49] Motivated by this new understanding and our recent example study, reductive unstable salts/solvents can be explored as Mg electrolytes if their decomposition product is tailored to form an SEI instead of a passivation layer. This opens the door to examining a vast amount of salts and solvents for designing Mg electrolytes with wide stability window, high ionic conductivity, and good compatibility with cathode materials.

METHODS

Electrochemistry. The carbon/sulfur composite electrode is prepared with the same procedure reported in our previous work.[31,32] Typical loading is 1 mg/cm^2, and carbon/sulfur ratio is ∼0.11. All Mg electrodes are polished by sandpaper to remove the surface oxide layer until a fresh and shining surface is exposed before electrochemical testing. Three-electrode Mg/S batteries were assembled for galvanostatic discharge/charge with sulfur/carbon composite as working electrode (WE), Mg disks as both reference electrode (RE) and counter electrode (CE), and $MgTFSI_2$−$MgCl_2$ complex as the electrolyte.[25] To avoid any ambiguity, discharge is defined as applying negative current on WE, and charge is defined as applying positive current on WE in our discussion. Electrolytes were prepared under pure argon atmosphere in MBraun, Inc. glovebox (<1 ppm of water and oxygen). $MgTFSI_2$(99.5%, Solvonic, France) was dried in vacuum at 240 °C for >10 h, and dimethoxyethane (DME, 99%, Sigma-Aldrich) was dried with molecular sieves for >24 h prior to use. Ultra dry $MgCl_2$(99.9%, Sigma-Aldrich) was directly used without further treatment. The electrolyte was prepared by adding $MgTFSI_2$ and $MgCl_2$ in the molar ratio of 1:2 in DME and stirring overnight. The molar concentration of the electrolyte is reported based on the amount of $MgTFSI_2$. For example, to make 0.25 M electrolyte, 0.25 M $MgTFSI_2$ and 0.5 M $MgCl_2$ was added to DME.

DOI: 10.1021/acsami.8b02425
ACS Appl. Mater. Interfaces XXXX, XXX, XXX−XXX

Material Characterization. SEM and EDX were conducted using a Hitachi SU-70 field emission scanning electron microscope. All the cycled Mg electrodes were fully washed with DME before EDX and XPS measurement. XPS was collected with a Kratos Axis 165 spectrometer operating in hybrid mode, using monochomatized Al Kα X-rays (1486.7 eV). Survey and high resolution spectra were collected with pass energies of 160 and 40 eV, respectively. Mg^0 (49.6 eV) is used as the reference to calibrate all the spectra. Peak fitting was done using CASA XPS software. Data were fit with a Shirley background using peaks with a 30% Lorentzian, 70% Gaussian product function. S 2p spectra were fit with spin−orbit split 2p 3/2 and 2p 1/2 doublets, constrained by 1.18 eV separation consistent with the spin−orbit splitting and a characteristic 2:1 area ratio. Cl 2p spectra were fit with spin−orbit split 2p 3/2 and 2p 1/2 doublets, constrained by 1.6 eV separation and a characteristic 2:1 area ratio.

■ ASSOCIATED CONTENT

Supporting Information

The Supporting Information is available free of charge on the ACS Publications website at DOI: 10.1021/acsami.8b02425.

Additional electrochemical data, SEM images, and EDX and XPS results (PDF)

■ AUTHOR INFORMATION

Corresponding Author

*E-mail: cswang@umd.edu.

ORCID

Tao Gao: 0000-0003-0204-3269

Chunsheng Wang: 0000-0002-8626-6381

Notes

The authors declare no competing financial interest.

■ ACKNOWLEDGMENTS

T.G. and C.W. acknowledge the support from the Nanostructures for Electrical Energy Storage (NEES), an Energy Frontier Research Center funded by the United States Department of Energy, Office of Science, Basic Energy Sciences, under Award DESC0001160. T.G. also acknowledges the Dean's Dissertation Fellowship from University of Maryland.

■ REFERENCES

(1) Yoo, H. D.; Shterenberg, I.; Gofer, Y.; Gershinsky, G.; Pour, N.; Aurbach, D. Mg Rechargeable Batteries: An on-Going Challenge. *Energy Environ. Sci.* **2013**, *6*, 2265−2279.

(2) Aurbach, D.; Lu, Z.; Schechter, a; Gofer, Y.; Gizbar, H.; Turgeman, R.; Cohen, Y.; Moshkovich, M.; Levi, E. Prototype Systems for Rechargeable Magnesium Batteries. *Nature* **2000**, *407*, 724−727.

(3) Canepa, P.; Sai Gautam, G.; Hannah, D. C.; Malik, R.; Liu, M.; Gallagher, K. G.; Persson, K. A.; Ceder, G. Odyssey of Multivalent Cathode Materials: Open Questions and Future Challenges. *Chem. Rev.* **2017**, *117*, 4287−4341.

(4) Bucur, C. B.; Gregory, T.; Oliver, A. G.; Muldoon, J. Confession of a Magnesium Battery. *J. Phys. Chem. Lett.* **2015**, *6*, 3578−3591.

(5) Sa, N.; Wang, H.; Proffit, D. L.; Lipson, A. L.; Key, B.; Liu, M.; Feng, Z.; Fister, T. T.; Ren, Y.; Sun, C.-J.; Vaughey, J. T.; Fenter, P. A.; Persson, K. A.; Burrell, A. K. Is Alpha-V2O5 a Cathode Material for Mg Insertion Batteries? *J. Power Sources* **2016**, *323*, 44−50.

(6) Sun, X.; Bonnick, P.; Duffort, V.; Liu, M.; Rong, Z.; Persson, K. A.; Ceder, G.; Nazar, L. F. A High Capacity Thiospinel Cathode for Mg Batteries. *Energy Environ. Sci.* **2016**, *9*, 2273−2277.

(7) Gao, P.; Zhao-karger, Z.; Mu, X.; Diemant, T.; Pfeifer, M.; Sai, V.; Chakravadhanula, K.; Behm, R. J. Interlayer-Expanded Vanadium Oxychloride as Electrode Material for Magnesium-Based Batteries. *ChemElectroChem* **2017**, *4*, 1−9.

(8) Incorvati, J. T.; Wan, L. F.; Key, B.; Zhou, D.; Liao, C.; Fuoco, L.; Holland, M.; Wang, H.; Prendergast, D.; Poeppelmeier, K. R.; Vaughey, J. T. Reversible Magnesium Intercalation into a Layered Oxyfluoride Cathode. *Chem. Mater.* **2016**, *28*, 17−20.

(9) Lipson, A. L.; Han, S.; Kim, S.; Pan, B.; Sa, N.; Liao, C.; Fister, T. T.; Burrell, A. K.; Vaughey, J. T.; Ingram, B. J. Nickel Hexacyanoferrate, a Versatile Intercalation Host for Divalent Ions from Nonaqueous Electrolytes. *J. Power Sources* **2016**, *325*, 646−652.

(10) Pan, B.; Huang, J.; Feng, Z.; Zeng, L.; He, M.; Zhang, L.; Vaughey, J. T.; Bedzyk, M. J.; Fenter, P.; Zhang, Z.; Burrell, A. K.; Liao, C. Polyanthraquinone-Based Organic Cathode for High-Performance Rechargeable Magnesium-Ion Batteries. *Adv. Energy Mater.* **2016**, *6*, 2−4.

(11) Zhang, R.; Yu, X.; Nam, K. W.; Ling, C.; Arthur, T. S.; Song, W.; Knapp, A. M.; Ehrlich, S. N.; Yang, X. Q.; Matsui, M. α-MnO 2 as a Cathode Material for Rechargeable Mg Batteries. *Electrochem. Commun.* **2012**, *23*, 110−113.

(12) Vardar, G.; Nelson, E. G.; Smith, J. G.; Naruse, J.; Hiramatsu, H.; Bartlett, B. M.; Sleightholme, A. E. S.; Siegel, D. J.; Monroe, C. W. Identifying the Discharge Product and Reaction Pathway for a Secondary Mg/O 2 Battery. *Chem. Mater.* **2015**, *27*, 7564−7568.

(13) Tian, H.; Gao, T.; Li, X.; Wang, X.; Luo, C.; Fan, X.; Yang, C.; Suo, L.; Ma, Z.; Han, W.; Wang, C. High Power Rechargeable Magnesium/iodine Battery Chemistry. *Nat. Commun.* **2017**, *8*, 14083.

(14) Gao, T.; Han, F.; Zhu, Y.; Suo, L.; Luo, C.; Xu, K.; Wang, C. Hybrid Mg2+/Li+ Battery with Long Cycle Life and High Rate Capability. *Adv. Energy Mater.* **2015**, *5*, 1401507.

(15) Cheng, Y.; Choi, D.; Han, K. S.; Mueller, K. T.; Zhang, J.; Sprenkle, V. L.; Liu, J.; Li, G. Toward the Design of High Voltage Magnesium-Lithium Hybrid Batteries Using Dual-Salt Electrolytes. *Chem. Commun.* **2016**, *52*, 5379−5382.

(16) Muldoon, J.; Bucur, C. B.; Oliver, A. G.; Sugimoto, T.; Matsui, M.; Kim, H. S.; Allred, G. D.; Zajicek, J.; Kotani, Y. Electrolyte Roadblocks to a Magnesium Rechargeable Battery. *Energy Environ. Sci.* **2012**, *5*, 5941−5950.

(17) Muldoon, J.; Bucur, C. B.; Gregory, T. Fervent Hype behind Magnesium Batteries: An Open Call to Synthetic Chemists - Electrolytes and Cathodes Needed. *Angew. Chem.* **2017**, *129*, 12232.

(18) Aurbach, D.; Gofer, Y.; Lu, Z.; Schechter, a.; Chusid, O.; Gizbar, H.; Cohen, Y.; Ashkenazi, V.; Moshkovich, M.; Turgeman, R. A Short Review on the Comparison between Li Battery Systems and Rechargeable Magnesium Battery Technology. *J. Power Sources* **2001**, *97−98*, 28−32.

(19) Gofer, Y.; Chusid, O.; Gizbar, H.; Viestfrid, Y.; Gottlieb, H. E.; Marks, V.; Aurbach, D. Improved Electrolyte Solutions for Rechargeable Magnesium Batteries. *Electrochem. Solid-State Lett.* **2006**, *9*, A257−A260.

(20) Zhao-Karger, Z.; Zhao, X.; Fuhr, O.; Fichtner, M. Bisamide Based Non-Nucleophilic Electrolytes for Rechargeable Magnesium Batteries. *RSC Adv.* **2013**, *3*, 16330−16335.

(21) Herb, J. T.; Nist-lund, C. A.; Arnold, C. B. A Fluorinated Alkoxyaluminate Electrolyte for Mag- Nesium-Ion Batteries. *ACS Energy Lett.* **2016**, *1*, 1−16.

(22) Tutusaus, O.; Mohtadi, R.; Arthur, T. S.; Mizuno, F.; Nelson, E. G.; Sevryugina, Y. V. An Efficient Halogen-Free Electrolyte for Use in Rechargeable Magnesium Batteries. *Angew. Chem., Int. Ed.* **2015**, *54*, 7900−7904.

(23) Zhao-Karger, Z.; Bardaji, E. G.; Fuhr, O.; Fichtner, M. New Class of Non-Corrosive, Highly Efficient Electrolytes for Rechargeable Magnesium Batteries. *J. Mater. Chem. A* **2017**, *5*, 1−6.

(24) Lu, Z.; Schechter, a.; Moshkovich, M.; Aurbach, D. On the Electrochemical Behavior of Magnesium Electrodes in Polar Aprotic Electrolyte Solutions. *J. Electroanal. Chem.* **1999**, *466*, 203−217.

(25) Shterenberg, I.; Salama, M.; Yoo, H. D.; Gofer, Y.; Park, J.-B.; Sun, Y.-K.; Aurbach, D. Evaluation of (CF3 SO2)2N- (TFSI) Based Electrolyte Solutions for Mg Batteries. *J. Electrochem. Soc.* **2015**, *162*, A7118−A7128.

(26) Connell, J. G.; Genorio, B.; Lopes, P. P.; Strmcnik, D.; Stamenkovic, V. R.; Markovic, N. M. Tuning the Reversibility of Mg

DOI: 10.1021/acsami.8b02425
ACS Appl. Mater. Interfaces XXXX, XXX, XXX−XXX

Anodes via Controlled Surface Passivation by H2O/Cl- in Organic Electrolytes. *Chem. Mater.* **2016**, *28*, 8268−8277.
(27) Rajput, N. N.; Qu, X.; Sa, N.; Burrell, A. K.; Persson, K. A. The Coupling between Stability and Ion Pair Formation in Magnesium Electrolytes from First-Principles Quantum Mechanics and Classical Molecular Dynamics. *J. Am. Chem. Soc.* **2015**, *137*, 3411−3420.
(28) Zhao-Karger, Z.; Zhao, X.; Wang, D.; Diemant, T.; Behm, R. J.; Fichtner, M. Performance Improvement of Magnesium Sulfur Batteries with Modified Non-Nucleophilic Electrolytes. *Adv. Energy Mater.* **2015**, *5*, 1401155.
(29) Yu, X.; Manthiram, A. Performance Enhancement and Mechanistic Studies of Room-Temperature Magnesium-Sulfur Batteries. *Chem. Mater.* **2016**, *28*, 896−905.
(30) Zhang, Z.; Cui, Z.; Qiao, L.; Guan, J.; Xu, H.; Wang, X.; Hu, P.; Du, H.; Li, S.; Zhou, X.; Dong, S.; Liu, Z.; Cui, G.; Chen, L. Novel Design Concepts of Efficient Mg-Ion Electrolytes toward High-Performance Magnesium-Selenium and Magnesium-Sulfur Batteries. *Adv. Energy Mater.* **2017**, *7*, 1602055.
(31) Gao, T.; Hou, S.; Wang, F.; Ma, Z.; Li, X.; Xu, K.; Wang, C. Reversible S0/MgSx Redox Chemistry in MgTFSI2-MgCl2 Electrolyte for Rechargeable Mg/S Battery. *Angew. Chem., Int. Ed.* **2017**, *56*, 13526.
(32) Gao, T.; Ji, X.; Hou, S.; Fan, X.; Li, X.; Yang, C.; Han, F.; Wang, F.; Jiang, J.; Xu, K.; Wang, C. Thermodynamics and Kinetics of Sulfur Cathode during Discharge in MgTFSI 2 −DME Electrolyte. *Adv. Mater.* **2018**, *30*, 1704313.
(33) Zhang, S. S. Liquid Electrolyte Lithium/sulfur Battery: Fundamental Chemistry, Problems, and Solutions. *J. Power Sources* **2013**, *231*, 153−162.
(34) Goodenough, J. B.; Park, K. S. The Li-Ion Rechargeable Battery: A Perspective. *J. Am. Chem. Soc.* **2013**, *135*, 1167−1176.
(35) Yoo, H. D.; Han, S.-D.; Bolotin, I. L.; Nolis, G. M.; Bayliss, R. D.; Burrell, A. K.; Vaughey, J. T.; Cabana, J. Degradation Mechanisms of Magnesium Metal Anodes in Electrolytes Based on (CF3SO2)2N− at High Current Densities. *Langmuir* **2017**, *33*, 9398−9406.
(36) Arthur, T. S.; Glans, A.; Singh, N.; Tutusaus, O.; Nie, K.; Liu, Y.-S.; Mizuno, F.; Guo, J.; Alsem, D. H.; Salmon, N. J.; Mohtadi, R. Interfacial Insight from Operando sXAS/TEM for Magnesium Metal Deposition with Borohydride Electrolytes. *Chem. Mater.* **2017**, *29*, 7183−7188.
(37) Fournier, V.; Marcus, P.; Olefjord, I. Oxidation of Magnesium. *Surf. Interface Anal.* **2002**, *34*, 494−497.
(38) Ardizzone, S.; Bianchi, C. L.; Fadoni, M.; Vercelli, B. Magnesium Salts and Oxide: An XPS Overview. *Appl. Surf. Sci.* **1997**, *119*, 253−259.
(39) Verdier, S.; Van Der Laak, N.; Delalande, S.; Metson, J.; Dalard, F. The Surface Reactivity of a Magnesium-Aluminium Alloy in Acidic Fluoride Solutions Studied by Electrochemical Techniques and XPS. *Appl. Surf. Sci.* **2004**, *235*, 513−524.
(40) Santamaria, M.; Di Quarto, F.; Zanna, S.; Marcus, P. Initial Surface Film on Magnesium Metal: A Characterization by X-Ray Photoelectron Spectroscopy (XPS) and Photocurrent Spectroscopy (PCS). *Electrochim. Acta* **2007**, *53*, 1314−1325.
(41) Mertin, S.; Marot, L.; Sandu, C. S.; Steiner, R.; Scartezzini, J. L.; Muralt, P. Nanocrystalline Low-Refractive Magnesium Fluoride Films Deposited by Reactive Magnetron Sputtering: Optical and Structural Properties. *Adv. Eng. Mater.* **2015**, *17*, 1652−1659.
(42) Wagner, C. D. *Handbook of X-Ray Photoelectron Spectroscopy*; Perkin-Elmer: Eden Prairie, 1979.
(43) Wagner, C. D. Studies of the Charging of Insulators in ESCA. *J. Electron Spectrosc. Relat. Phenom.* **1980**, *18*, 345−349.
(44) Garbassi, F.; Pozzi, L. Electron Beam Effects on Hydrated Magnesium Chloride Revealed by XPS. *J. Electron Spectrosc. Relat. Phenom.* **1979**, *16*, 199−203.
(45) Magni, E.; Somorjai, G. A. Electron-Irradiation-Induced Reduction of Magnesium-Chloride Thin-Films Deposited on Gold - Xps and Iss Study. *Surf. Sci.* **1995**, *341*, L1078−L1084.
(46) Dedryvère, R.; Leroy, S.; Martinez, H.; Blanchard, F.; Lemordant, D.; Gonbeau, D. XPS Valence Characterization of Lithium Salts as a Tool to Study Electrode/electrolyte Interfaces of Li-Ion Batteries. *J. Phys. Chem. B* **2006**, *110*, 12986−12992.
(47) Suo, L.; Borodin, O.; Gao, T.; Olguin, M.; Ho, J.; Fan, X.; Luo, C.; Wang, C.; Xu, K. Water-in-Salt " Electrolyte Enables High-Voltage Aqueous Lithium-Ion Chemistries. *Science* **2015**, *350*, 938−943.
(48) Baskin, A.; Prendergast, D. Exploration of the Detailed Conditions for Reductive Stability of Mg(TFSI) 2 in Diglyme: Implications for Multivalent Electrolytes. *J. Phys. Chem. C* **2016**, *120*, 3583−3594.
(49) Li, X.; Gao, T.; Han, F.; Ma, Z.; Fan, X.; Hou, S.; Eidson, N.; Li, W.; Wang, C. Reducing Mg Anode Overpotential via Ion Conductive Surface Layer Formation by Iodine Additive. *Adv. Energy Mater.* **2018**, *8*, 1701728.

DOI: 10.1021/acsami.8b02425
ACS Appl. Mater. Interfaces XXXX, XXX, XXX−XXX